Prism Inside: Spectroscopic and Magnetic Properties of the Lanthanide(III) Chloride Oxidotungstates(VI) $Ln_3Cl_3[WO_6]$ (Ln = La – Nd, Sm – Tb)

Katharina V. Dorn,[a] Björn Blaschkowski,[a] Katharina Förg,[b] Philip Netzsch,[b] Henning A. Höppe,[b] and Ingo Hartenbach*[a]

Dedicated to Professor Wolfgang Schnick on the Occasion of his 60th Birthday

Abstract. The lanthanide(III) chloride oxidotungstates(VI) with the formula $Ln_3Cl_3[WO_6]$ for Ln = La – Nd, Sm – Tb were synthesized by solid-state reactions utilizing the respective lanthanide trichloride, lanthanide sesquioxide (where available), and tungsten trioxide together with lithium chloride as flux. The title compounds crystallize hexagonally in space group $P6_3/m$ (no. 176, a = 941–909, c = 543–525 pm, Z = 2). The structures comprise crystallographically unique Ln^{3+} cations surrounded by six O^{2-} and four Cl^- anions (C.N. = 10) forming distorted tetracapped trigonal prisms as well as rather uncommon trigonal prismatic $[WO_6]^{6-}$ units, whose edges are coordinated by nine Ln^{3+} cations. Thus, a $^3_\infty\{([WO_6]Ln^e_{9/3})^{3+}\}$ framework (e = edge-sharing) is created, which contains tube-shaped channels along [001] lined with chloride anions. To elucidate the spectroscopic and magnetic properties of the obtained pure phase samples, single-crystal Raman (for Ln = La – Nd, Sm–Tb), diffuse reflectance (for Ln = La, Pr, Nd, Gd), and luminescence spectroscopy (for bulk $Ln_3Cl_3[WO_6]$ (Ln = La, Eu, Gd, Tb) and Eu^{3+}- or Tb^{3+}-doped derivatives of $La_3Cl_3[WO_6]$ and $Gd_3Cl_3[WO_6]$, respectively) were performed and their temperature-dependent magnetic moments (for Ln = Pr, Nd, Gd) were determined.

Introduction

In this day and age, investigations in order to synthesize, characterize, and optimize energy-efficient materials play an important role all over the world and their demand is more and more increasing. This includes research in the area of luminescent materials for low-energy illumination. An interesting class of compounds for this endeavour is represented by rare-earth metal(III) oxidotungstates(VI) and their anionic derivatives, since these materials make use of the $O^{2-} \rightarrow W^{6+}$ ligand-to-metal charge transfer (LMCT) as sensitizer to deliver the harvested energy to active centers (e.g. Eu^{3+}, Tb^{3+}…) in the crystal structure ("inorganic antenna effect").[1,2] This mechanism usually provides a broad energy band and is thus able to serve a wider range of excitation energies than the direct f–f excitation of the luminescence-active lanthanide(III) cations mentioned before, since this takes only place at one single wavelength.[3] In case of the oxidotungstate(VI) derivatives there is a wide diversity of suitable host lattices,[4] bearing different anions such as tetrahedral $[WO_4]^{2-}$,[2,5–10] trigonal-bipyramidal or square pyramidal $[WO_5]^{4-}$ units,[11] as well as condensed iso- or heteropolytungstate entities.[12] Isolated $[WO_6]^{6-}$ octahedra[13] are almost as rarely found in crystal structures as trigonal prismatic units with the same formula, however in lanthanide chemistry compounds of the formula $Ln_3Cl_3[WO_6]$, containing the aforementioned $[WO_6]^{6-}$ prisms are obtained for the larger Ln^{3+} cations. With $Pr_3Cl_3[WO_6]$ being the first lanthanide(III) chloride oxidotungstate(VI) that founds entry into literature,[14] *Brixner* et al. performed thorough research on $La_3Cl_3[WO_6]$ more than 30 years ago, including luminescence investigations on doped compounds.[15–17] The aforementioned publications also comprise mentions about lattice constants of the $Ln_3Cl_3[WO_6]$ representatives for Ln = La – Nd and Sm – Gd. A decade later luminescence properties of Pr^{3+}- and Eu^{3+}-doped $La_3Cl_3[WO_6]$ were again investigated by *Cascales* et al.[18,19] and one of the reasons for a high interest in this system is the fact that an enlarged coordination number around the W^{6+} cations causes a significant shift of the maximum for the LMCT band in the excitation spectrum towards longer wavelengths (= lower energies) with respect to the value found from tetrahedral $[WO_4]^{2-}$ entities.

In this paper details on investigations of the crystal structures for the $Ln_3Cl_3[WO_6]$ representatives with Ln = Nd, Sm – Tb are given for the first time, with $Tb_3Cl_3[WO_6]$[20] being the derivative with the smallest Ln^{3+} in this series, obtainable by solid-state reactions (crystallographic data for the La, Ce, and Pr representatives were recorded to present the whole series with the larger lanthanides). Furthermore, single-crystal Raman spectra were taken and comprehensively com-

* Dr. I. Hartenbach
E-Mail: hartenbach@iac.uni-stuttgart.de
[a] Institute for Inorganic Chemistry
University of Stuttgart
Pfaffenwaldring 55
70563 Stuttgart, Germany
[b] Institute for Physics
University of Augsburg
Universitätsstraße 1
86159 Augsburg, Germany
Supporting information for this article is available on the WWW under **http://dx.doi.org/10.1002/zaac.201700247** or from the author.

pared to other tungstate compounds. Since former publications on the $Ln_3Cl_3[WO_6]$ family of compounds focused on the suitability of the lanthanum derivative as host material for luminescence applications, this work concentrates on spectroscopic investigations of $Gd_3Cl_3[WO_6]$ as well as Eu^{3+}- and Tb^{3+}-doped samples thereof.

Results and Discussion

Crystal Structure

The lanthanide(III) chloride oxidotungstate(VI) representatives with the formula $Ln_3Cl_3[WO_6]$ (*Ln* = La – Nd, Sm – Tb) crystallize hexagonally in space group $P6_3/m$ (no. 176) exhibiting lattice parameters in the ranges of a = 941–909 pm, c = 543–525 pm and two formula units per unit cell (see Table 1 for details). Their well-known crystal structures are isotypic to those of $La_3Cl_3[WO_6]$,[15,17] $Ce_3Cl_3[WO_6]$,[21] and $Pr_3Cl_3[WO_6]$,[14] comprising crystallographically unique Ln^{3+} cations, which are coordinated by six O^{2-} and four Cl^- anions forming distorted tetracapped trigonal prisms (see Figure 1). The interatomic distances between the Ln^{3+} cations and all enclosing anions reside in the usual range found in other compounds bearing the respective ions. Even for Tb^{3+}, the smallest lanthanide in this series, there is no detachment tendency for either of the surrounding anions detectable, thus, a coordination number of ten is maintained. The hexavalent tungsten cations are surrounded by six O^{2-} anions building up

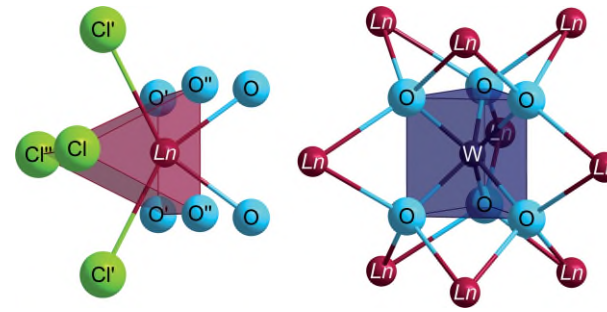

Figure 1. Distorted tetracapped trigonal prism of Cl^- and O^{2-} anions around the Ln^{3+} cations (left) and trigonal prismatic coordination of the W^{6+} cations formed by six O^{2-} anions with each edge capped by one Ln^{3+} cation building a tetracaidecadeltahedron (right) in the structure of the $Ln_3Cl_3[WO_6]$ representatives (*Ln* = La – Nd, Sm – Tb).

Table 1. Crystal structure data for the hexagonal $Ln_3Cl_3[WO_6]$ representatives (*Ln* = La – Nd, Sm – Tb).

Lanthanide	La	Ce[21]	Pr	Nd	Sm	Eu	Gd	Tb
Crystal system	hexagonal							
Space group	$P6_3/m$ (no. 176)							
Formula units /Z	2							
a /pm	940.85(4)	934.30(4)	928.49(4)	925.55(4)	918.02(4)	914.68(4)	912.60(4)	908.56(4)
c /pm	542.72(2)	539.05(2)	535.83(2)	534.06(2)	529.85(2)	528.15(2)	526.66(2)	524.63(2)
c/a ratio	0.5768	0.5770	0.5771	0.5770	0.5772	0.5774	0.5771	0.5774
Density D_x /g·cm^{-3}	6.409	6.573	6.716	6.864	7.190	7.308	7.501	7.642
Molar volume V_m /cm^3·mol^{-1}	125.28	122.70	120.46	119.30	116.44	115.23	114.38	112.93
$F(000)$	688	694	700	706	718	724	730	736
Index range, $\pm h/\pm k/\pm l$	13/13/7	14/14/8	12/12/6	12/12/6	12/11/6	12/12/6	11/11/6	11/11/6
$2\theta_{max}$ /°	60.43	65.14	55.57	55.49	55.44	55.58	55.17	55.42
Absorption coefficient μ /mm^{-1}	29.818	31.474	33.261	34.795	38.286	40.259	41.978	44.276
Data corrections	Background, polarization and Lorentz factors, numerical absorption correction by the program HABITUS[22]							
Reflections collected / unique	8900 / 464	10378 / 548	5751 / 346	5201 / 341	3593 / 333	4841 / 331	5331 / 329	3341 / 329
Refined parameters	25							
R_{int}/R_σ	0.097/0.026	0.094/0.024	0.103/0.029	0.092/0.025	0.088/0.037	0.113/0.042	0.070/0.021	0.076/0.034
Structure solution and refinement	Program package SHELX-2013 [23] scattering factors according to International Tables, Vol. C [24]							
R_1 for (n) reflections with $\lvert F_o\rvert \geq 4\sigma(F_o)$	0.019 (455)	0.019 (546)	0.020 (342)	0.017 (339)	0.022 (300)	0.022 (295)	0.015 (327)	0.020 (303)
R_1 / wR_2 for all reflections	0.020 / 0.048							
Goodness of Fit (GooF)	1.138	1.160	1.134	1.142	1.000	1.006	1.206	0.993
Extinction, g	0.093(3)	0.146(3)	0.084(3)	0.079(2)	0.0049(3)	0.0021(4)	0.018(1)	0.0033(3)
Residual electron density ρ /e$^-$·10^{-6} pm^{-3}, min / max	–1.80 / 1.60	–2.24 / 3.50	–1.64 / 1.86	–1.19 / 1.14	–1.63 / 1.30	–1.23 / 1.31	–1.14 / 0.90	–1.30 / 1.25
ICSD number	430854	420130	430855	430856	430857	430859	430858	430860

rather uncommon isolated trigonal prismatic $[WO_6]^{6-}$ entities exhibiting W^{6+}–O^{2-} bond lengths between 192 and 194 pm, which are common values for hexavalent tungsten coordinated by six oxide anions. All nine edges of those prisms are capped by one lanthanide cation each, creating a $^3_\infty\{([WO_6]Ln^e_{9/3})^{3+}\}$ framework (*e* = edge-sharing) with void tube-shaped channels along [001], which are lined by chloride anions (see Figure 2).

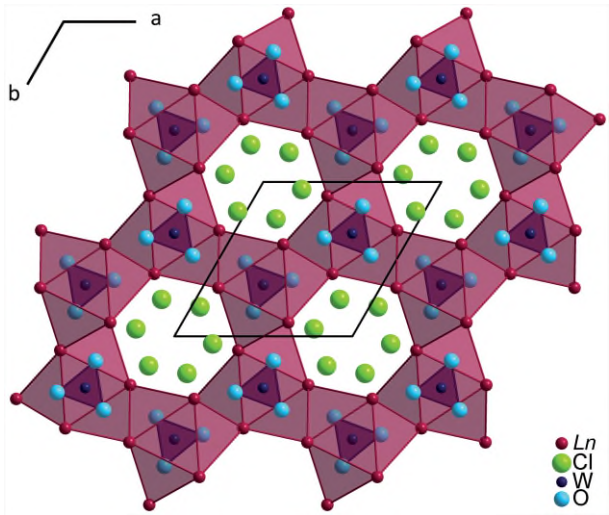

Figure 2. View at the expanded hexagonal unit cell of the $Ln_3Cl_3[WO_6]$ representatives (*Ln* = La – Nd, Sm – Tb) along the *c* axis, emphasizing the trigonal prisms $[WO_6]^{6-}$ (dark blue), the $^3_\infty\{([WO_6]Ln^e_{9/3})^{3+}\}$ framework (*e* = edge-sharing) (purple) and the tube-shaped channels along [001] formed by the Cl^- anions.

Single-Crystal Raman Spectroscopy

Brixner et al. investigated the Raman spectrum of $La_3Cl_3[WO_6]$[15] and indicated the vibration modes for this compound using a green laser (λ = 514.5 nm) to be found at 204, 225, 364, 484, 550, 558, and 777 cm^{-1}. Based on the D_{3h} point symmetry of the $[WO_6]^{6-}$ unit seven Raman-active modes are expected in the spectrum (2 A_1' + 3 E' + 2 E''). Recent investigations of all the $Ln_3Cl_3[WO_6]$ derivatives for *Ln* = La – Nd, Sm – Tb show equivalent results, in which the modes emerge in a range between 200 and 800 cm^{-1} as well (see Figure 3).

Vibrational modes of the crystal lattice as well as Ln^{3+}–O^{2-} vibrations are attributed to the bands with lower wavenumbers. Due to the slightly decreasing interatomic distances from $La_3Cl_3[WO_6]$ being the representative with the largest Ln^{3+} cation to $Tb_3Cl_3[WO_6]$ bearing the smallest Ln^{3+} cation within the discussed series, these latter modes are shifted towards higher wavenumbers throughout the series. The comparison of the single-crystal Raman spectra of the $Ln_3Cl_3[WO_6]$ representatives for *Ln* = La – Nd, Sm – Tb to minerals presented by the *RRUFF* project[25] exhibits the differences between the trigonal prismatic $[WO_6]^{6-}$ units, which are unique for these structures, and (distorted) tetrahedral or octahedral oxygen coordination spheres for tungsten(VI) cations known from minerals such as *stolzite* ($Pb[WO_4]$, R050568), *scheelite* ($Ca[WO_4]$, R040172), *raspite* (α-$PbWO_4$, R050567), *hübnerite* ($MnWO_4$, R050069), and *ferberite* ($FeWO_4$, R050090). The ranges for the Raman modes of the title compounds are detected to be lower in general as those in the aforementioned minerals (see Figure 4).

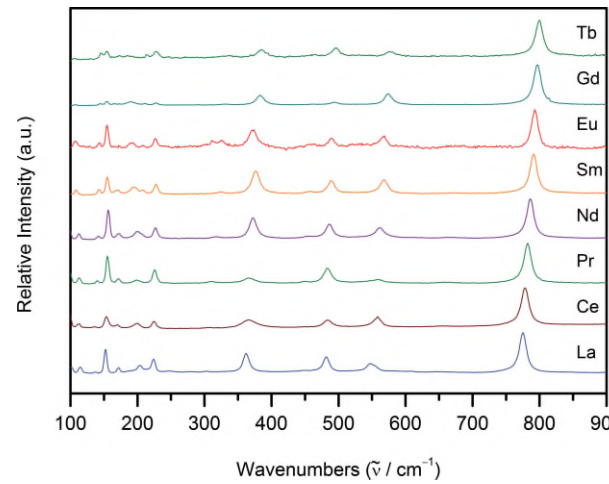

Figure 3. Single-crystal Raman spectra of the hexagonal $Ln_3Cl_3[WO_6]$ representatives (*Ln* = La – Nd, Sm – Tb) (from bottom to top).

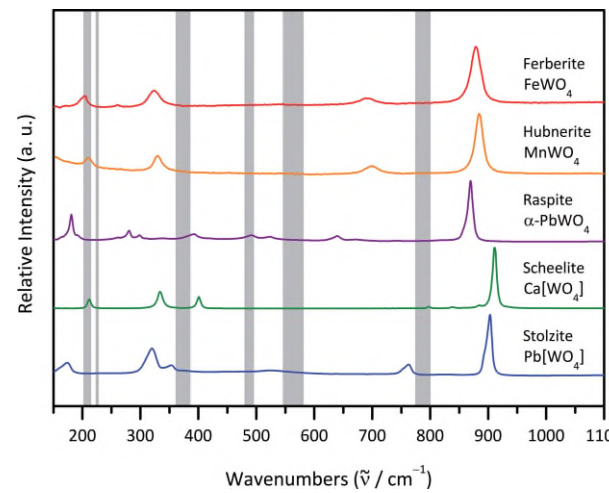

Figure 4. Single-crystal Raman spectra of the minerals *stolzite* ($Pb[WO_4]$, *t*), *scheelite* ($Ca[WO_4]$, *t*), *raspite* (α-$PbWO_4$, *o*), *hübnerite* ($MnWO_4$, *o*) and *ferberite* ($FeWO_4$, *o*) (from bottom to top) in comparison to the ranges of the Raman modes for the title compounds $Ln_3Cl_3[WO_6]$ (grey marked areas, *tp*) (*t* = tetrahedral units, *o* = toctahedral units, *tp* = trigonal prismatic units).

The strongest peaks, the symmetric stretching vibration modes, shift from higher wavenumbers (around 900 cm^{-1}) for the tetrahedral $[WO_4]^{2-}$ units found in *stolzite* and *scheelite* via slightly lower ones (around 850 cm^{-1}) for the minerals *raspite*, *hübnerite*, and *ferberite* bearing octahedral units to even lower wavenumbers (less than 800 cm^{-1}) for the discussed trigonal prismatic $[WO_6]^{6-}$ units in the title compounds.

Diffuse Reflectance and Luminescence Spectroscopy

The diffuse reflectance spectra of the lanthanide(III) chloride oxidotungstates(VI) with the formula $Ln_3Cl_3[WO_6]$ (*Ln* =

La, Pr, Nd, Gd) were recorded from powdered bulk substances comprising linear fits to the detected curve in order to estimate the optical bandgaps for the respective compounds (Table 2; Figures S1–S4, Supporting Information). The optical bandgap for all four investigated materials are found within the near UV region of the electromagnetic spectrum. In addition to the optical bandgap, f–f transitions of the Pr^{3+} cations are visible between 2.06 eV and 2.77 eV (Figure S1, Supporting Information), whereas the respective transitions of the neodymium compound occur in the range of 1.41 eV to 3.54 eV (Figure S2, Supporting Information). Excitation with UV light induces luminescence in bulk samples of $Eu_3Cl_3[WO_6]$ and $Tb_3Cl_3[WO_6]$ (Figures S5 and S6, Supporting Information) as well as in the Eu^{3+}- or Tb^{3+}-doped $Ln_3Cl_3[WO_6]$ derivatives with *Ln* = La (Figures S7–S9, Supporting Information) and Gd. Since activator doped $La_3Cl_3[WO_6]$ materials were already researched in detail[8,15,16,18,19,26] this investigation focusses on undoped $Gd_3Cl_3[WO_6]$ and its Eu^{3+}- and Tb^{3+}-doped derivatives. In contrast to the pure gadolinium compound, which exclusively shows white light charge-transfer transitions of the trigonal prismatic $[WO_6]^{6-}$ units by excitation under UV light (Figure 5), the compounds containing Eu^{3+} and Tb^{3+} reveal emissions in the red and green spectral region, respectively. The broad excitation bands around 250–350 nm found in both, the Eu^{3+}- and Tb^{3+}-doped $Gd_3Cl_3[WO_6]$ (as well as in the undoped compound, see Figure 5, Figure 6, and Figure 7) represent the $O^{2-} \rightarrow W^{6+}$ LMCT, which shifted significantly towards lower energies compared to compounds bearing isolated $[WO_4]^{2-}$ units.[3,5]

Table 2. Optical bandgaps of the investigated $Ln_3Cl_3[WO_6]$ representatives (*Ln* = La, Pr, Nd, Gd).

Compound	*E* /eV	$\tilde{\nu}$ /1000 cm^{-1}	λ /nm
$La_3Cl_3[WO_6]$	3.84	31.0	323
$Pr_3Cl_3[WO_6]$	3.34	26.9	371
$Nd_3Cl_3[WO_6]$	3.66	29.5	339
$Gd_3Cl_3[WO_6]$	3.65	29.4	340

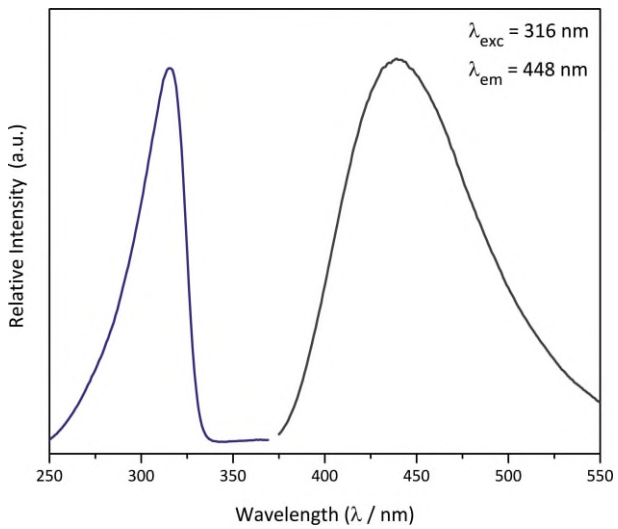

Figure 5. Excitation (blue, left) and emission spectrum (grey, right) of undoped $Gd_3Cl_3[WO_6]$ at a temperature of 77 K.

The emission spectrum of $Gd_3Cl_3[WO_6]:Eu^{3+}$ exhibits the typical bands for Eu^{3+} residing at a *non*-centrosymmetric position, i.e. the electric dipole $^5D_0 \rightarrow {}^7F_2$ transition represents the strongest peak (Figure 6).[27,28] The same is true for the emission spectrum of $Gd_3Cl_3[WO_6]:Tb^{3+}$, which receives its bright green color from the $^5D_4 \rightarrow {}^7F_5$ transition being its highest peak (Figure 7).[28,29]

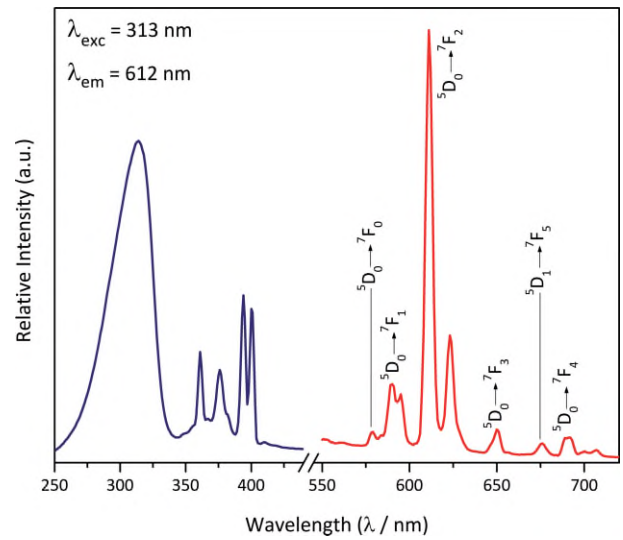

Figure 6. Excitation (blue, left) and emission spectrum (red, right) of $Gd_3Cl_3[WO_6]:Eu^{3+}$ at a temperature of 77 K.

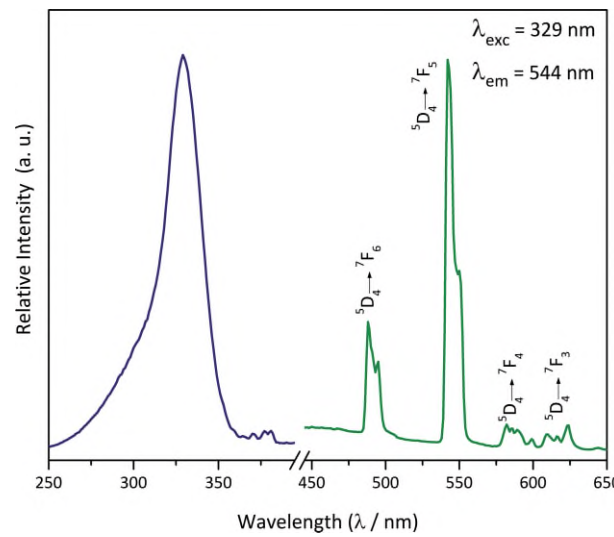

Figure 7. Excitation (blue, left) and emission spectrum (green, right) of $Gd_3Cl_3[WO_6]:Tb^{3+}$ at a temperature of 77 K.

Measurements of Magnetic Properties

As the involved lanthanide(III) cations exhibit interatomic distances of at least 400 pm no direct Ln^{3+}–Ln^{3+} magnetic interactions are expected. At temperatures higher than 150 K all three investigated $Ln_3Cl_3[WO_6]$ representatives, $Pr_3Cl_3[WO_6]$, $Nd_3Cl_3[WO_6]$, and $Gd_3Cl_3[WO_6]$ revealed typical Curie or Curie-Weiss behavior, respectively, showing magnetic mo-

ments μ_{exp} close to their theoretical values μ_{eff} (Figure 8 and Figure 9). $Gd_3Cl_3[WO_6]$ shows an almost perfect Curie behavior over the whole measured temperature range, the magnetic moment of the Gd^{3+} cations was determined to μ_{exp} = 7.96(1) μ_B which matches the theoretical value of μ_{eff} = 7.94 μ_B nearly perfect. The Weiss constant of Θ = 0.7(1) K for $Gd_3Cl_3[WO_6]$ indicates that no dominant magnetic interactions between the highly paramagnetic Gd^{3+} cations emerge.

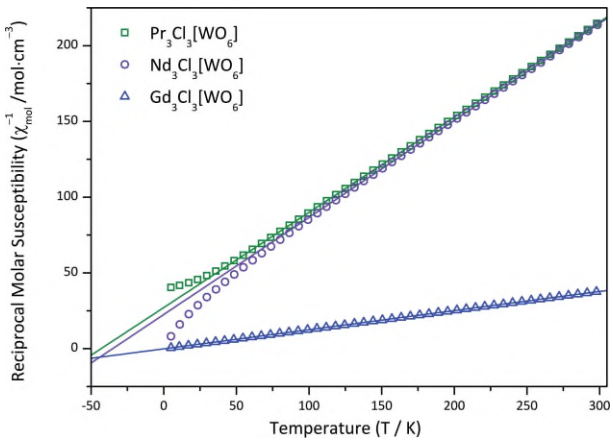

Figure 8. Reciprocal values of the molar magnetic susceptibilities $1/\chi_{mol}$ for three $Ln_3Cl_3[WO_6]$ representatives (*Ln* = Pr, Nd and Gd).

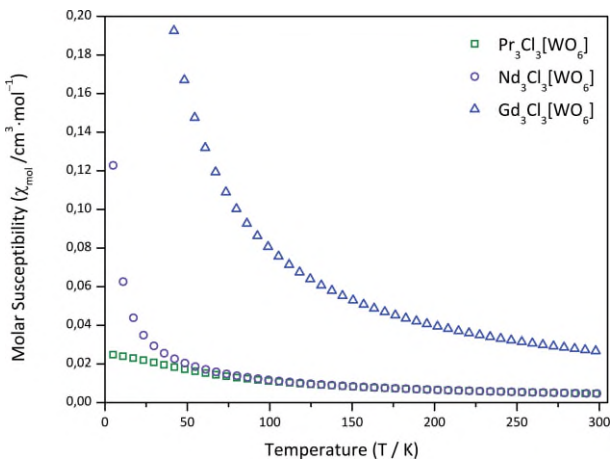

Figure 9. Molar magnetic susceptibilities χ_{mol} for three $Ln_3Cl_3[WO_6]$ representatives (*Ln* = Pr, Nd and Gd).

For $Pr_3Cl_3[WO_6]$ and $Nd_3Cl_3[WO_6]$ Curie-Weiss behavior with Weiss constants of Θ = –43(1) K for the praseodymium and –35(1) K for the neodymium representative, respectively, was found, which indicates a predominant influence of their crystal fields in the examined temperature range. In the latter cases, also significant deviations from the ideal linear relationship between $1/\chi_{mol}$ and *T* were observed for temperatures below 100 K (Figure 8). Their experimentally determined magnetic moments with μ_{exp} = 3.57(1) μ_B for $Pr_3Cl_3[WO_6]$ and μ_{exp} = 3.53(1) μ_B for $Nd_3Cl_3[WO_6]$ were also found to be very close to their theoretical values of μ_{eff} = 3.58 μ_B and μ_{eff} = 3.62 μ_B , respectively. While in $Pr_3Cl_3[WO_6]$ the deviation from the linear $1/\chi_{mol}$ vs. *T* relation below 50 K manifests in a way that higher values of $1/\chi_{mol}$ were obtained, the contrary was observed for the neodymium compound. Here the curve is bend towards lower values of $1/\chi_{mol}$ (Figure 8). These findings confirm earlier measurements on other trivalent praseodymium and neodymium compounds and theoretical calculations addressed them to the splitting of the ground states associated with Pr^{3+} and Nd^{3+} cations under the influence of their crystal fields.[26,30,31]

Conclusions

In this article the synthesis and crystal structures of the lanthanide(III) chloride oxidotungstate(VI) representatives with the formula $Ln_3Cl_3[WO_6]$ are described for *Ln* = La – Nd, Sm – Tb, which quite extraordinarily contain isolated trigonal prismatic $[WO_6]^{6-}$ entities. Data from single crystal Raman spectroscopy were recorded and discussed with special focus on vibrations emerging from the aforementioned trigonal $[WO_6]^{6-}$ prisms in comparison to compounds with tetrahedral and octahedral oxidotungstate units. Furthermore, an extensive investigation on luminescence properties of Eu^{3+}- and Tb^{3+}-doped samples of $Gd_3Cl_3[WO_6]$ was carried out. Finally, the magnetic characteristics of the $Ln_3Cl_3[WO_6]$ derivatives with *Ln* = Pr, Nd and Gd were investigated, their experimental magnetic moments were determined, and from Curie-Weiss law divergent behavior was discussed. Due to the straightforward synthesis route leading to single-phase materials and their ability of hosting active cations, the series of lanthanide(III) chloride oxidotungstate(VI) representatives $Ln_3Cl_3[WO_6]$ with *Ln* = La – Nd, Sm – Tb can be considered as highly interesting materials for further investigations regarding luminescence applications.

Experimental Section

Synthetic Procedures: By annealing equivalent amounts of lanthanide trichloride ($LnCl_3$: *Ln* = La, Nd, Sm, 99.9 %, ChemPur, Karlsruhe, Germany; *Ln* = Pr, Gd, 99.9 %, Heraeus, Hanau, Germany; *Ln* = Eu, 99.9 %, Sigma Aldrich, Taufkirchen, Germany), lanthanide sesquioxide (Ln_2O_3: *Ln* = La, Nd, Sm, Gd, 99.9 %, ChemPur, Karlsruhe, Germany; *Ln* = Eu, 99.999 %, Alfa Aesar, Karlsruhe, Germany), and tungsten trioxide (WO_3: 99.9 %, Merck, Darmstadt, Germany) in evacuated and fused silica ampoules for 3 d at 650–750 °C single crystals as well as microcrystalline powders of the $Ln_3Cl_3[WO_6]$ representatives with *Ln* = La – Nd, Sm – Tb were obtained (see Equation 1).

$$LnCl_3 + Ln_2O_3 + WO_3 \rightarrow Ln_3Cl_3[WO_6] \quad (1)$$

Lithium chloride (LiCl: 99.9 %, ChemPur, Karlsruhe, Germany) or an excess of the respective lanthanide chloride $LnCl_3$ served as fluxing agents in this solid-state reactions, which could be removed easily by washing with water. Since the sesquioxides of cerium, praseodymium, and terbium are not commercially available, they were produced in situ by synproportionation of the respective lanthanide(IV) or lanthanide(III,IV) oxides (CeO_2, Pr_6O_{11}, Tb_4O_{11}: 99.9 %, ChemPur, Karlsruhe, Germany) and the metals (Ce, Pr, Tb: 99.9 %, ChemPur, Karlsruhe, Germany). The obtained crystals were needle- or lath-shaped (Figure S10, Supporting Information), but hexagonal plates or prisms were also identified in the bulk products. Their colors correspond to those typical for the respective lanthanide trications Ln^{3+} (col-

orless for *Ln* = La, Eu, Gd, Tb; green for *Ln* = Pr; pale lilac for *Ln* = Nd; pale yellow for *Ln* = Sm). The observed red color of the cerium compound is due to the fact that the transition energy of Ce^{3+} is often found to be lowered depending on its chemical surrounding. Therefore it can be assigned to the effect that the f-electron containing orbital is located within the bandgap between the conduction and valence band.[28,32]

A second pathway to obtain the title compounds was generated by the chemical reaction of lanthanide(III) oxide chlorides *Ln*OCl for the examples of *Ln* = Pr and Nd with tungsten trioxide, in which the lanthanide(III) oxide chlorides were obtained by mixing praseodymium trichloride, hexapraseodymium undecaoxide, and praseodymium metal in molar ratios of 11:3:4 or equivalent amounts of neodymium trichloride and neodymium sesquioxide, respectively. The mixtures were heated in fused and evacuated silica ampoules at 650 °C for 3 d.

For the synthesized Eu^{3+}- and Tb^{3+}-doped compounds about 1 % of europium sesquioxide or terbium chloride, respectively, were added replacing the adequate share of the optically neutral components in the reaction mixtures of the intended host materials $La_3Cl_3[WO_6]$ and $Gd_3Cl_3[WO_6]$, respectively. All obtained compounds remained inert to atmospheric conditions and temperatures up to 850 °C.

Single-crystal X-ray Structure Determination: Intensity data sets for the single crystals of the hexagonal compounds with the formula $Ln_3Cl_3[WO_6]$ (*Ln* = La – Nd, Sm – Tb) were collected with a Nonius Kappa-CCD (Bruker AXS, Karlsruhe, Germany) single-crystal diffractometer by using graphite-monochromated Mo-K_α radiation (λ = 71.07 pm). In all cases numerical absorption corrections as well as the crystal structure solutions and refinements were performed with the program HABITUS and the program package SHELX-97/2013, respectively.[22,23] The crystal structure data are displayed in Table 1.

Further details of the crystal structures investigations may be obtained from the Fachinformationszentrum Karlsruhe, 76344 Eggenstein-Leopoldshafen, Germany (Fax: +49-7247-808-666; E-Mail: crysdata@fiz-karlsruhe.de, http://www.fiz-karlsruhe.de/request for deposited data.html) on quoting the depository numbers CSD-430854 ($La_3Cl_3[WO_6]$), CSD-420130 ($Ce_3Cl_3[WO_6]$)[21], CSD-430855 ($Pr_3Cl_3[WO_6]$), CSD-430856 ($Nd_3Cl_3[WO_6]$), CSD-430857 ($Sm_3Cl_3[WO_6]$), CSD-430859 ($Eu_3Cl_3[WO_6]$), CSD-430858 ($Gd_3Cl_3[WO_6]$), and CSD-430860 ($Tb_3Cl_3[WO_6]$).

X-ray Powder Diffraction: For all powder samples of the $Ln_3Cl_3[WO_6]$ series (*Ln* = La – Nd, Sm – Tb) the X-ray diffraction intensity data sets were recorded with a Stoe STADI P diffractometer (Stoe & Cie, Darmstadt, Germany) equipped with a germanium-monochromated Cu-K_α radiation (λ = 154.06 pm) and an image plate or position-sensitive detector, respectively. The data were evaluated with the program STOE WinXPOW 3.04.[33] The Rietveld refined diffractogram of $La_3Cl_3[WO_6]$ is shown in Figure 10 as an example for the single-phase bulk products of the $Ln_3Cl_3[WO_6]$ representatives.[34] A comparison between the measured powder diffractograms and calculated X-ray powder patterns obtained by single-crystal XRD for all materials that were involved in spectroscopic or magnetic measurements are given in Figure S11 (Supporting Information).

Raman Spectroscopy: Single-crystal Raman spectroscopy for the $Ln_3Cl_3[WO_6]$ representatives with *Ln* = La – Nd, Sm – Tb was performed with the help of a Horiba XploRa spectrometer using a LASER device with a wavelength of λ = 638 nm.

Diffuse Reflectance Spectroscopy: Diffuse reflectance spectra (DRS) of the hexagonal $Ln_3Cl_3[WO_6]$ compounds (*Ln* = La, Pr, Nd, Gd) were recorded by a J&M TIDAS UV/Vis/NIR spectrophotometer (J&M Analytik AG, Essingen, Germany), which was equipped to measure diffuse scattered radiation. As standard white reference barium sulfate ($Ba[SO_4]$) was used and the Kubelka-Munk function was applied in order to obtain band-gap information of the respective compounds.[35–37] The calculated band-gaps are listed in Table 2.

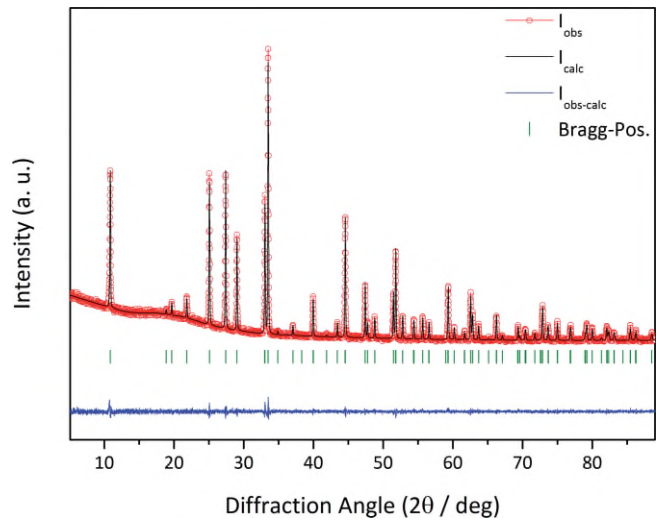

Figure 10. Rietveld refined powder diffractogram of $La_3Cl_3[WO_6]$ as representative for the $Ln_3Cl_3[WO_6]$ (*Ln* = La – Nd, Sm – Tb) series.

Luminescence Spectroscopy: For measuring the solid-state excitation and emission spectra of bulk $Eu_3Cl_3[WO_6]$ and $Tb_3Cl_3[WO_6]$ as well as for Eu^{3+}- and Tb^{3+}-doped $Ln_3Cl_3[WO_6]$ (*Ln* = La, Gd), respectively, a Horiba FluoroMax-4 (Horiba, Kyoto, Japan) fluorescence spectrometer was used for scanning a range between 200 and 800 nm with a xenon discharge lamp at a temperature of 77 K. The assignment of the electronic transitions resulted from the energy-level diagrams for the trivalent europium and terbium cations (see Figure 6 and Figure 7, as well as Figures S5, S6, S8, and S9, Supporting Information).

Measurements of Magnetic Properties: Between 50 and 70 mg of polycrystalline samples of $Ln_3Cl_3[WO_6]$ (*Ln* = Pr, Nd, Gd) were placed into gelatine capsules and attached on the sample holder of a Vibrating Sample Magnetometer (VSM) for measuring the magnetization *M*(T) in a Magnetic Property Measurement System (Quantum Design MPMS3, San Diego, CA, USA). The samples were examined in the temperature range of 5 to 300 K in a homogeneous magnetic field of 250 Oe. From these temperature-dependent data the molar magnetic susceptibilities χ_{mol} and their inverse values $1/\chi_{mol}$ for the $Ln_3Cl_3[WO_6]$ representatives (*Ln* = Pr, Nd, Gd) were calculated.

Supporting Information (see footnote on the first page of this article): The supporting information contains diffuse reflectance and photoluminescence spectra of several doped and undoped $Ln_3Cl_3[WO_6]$ representatives, a picture of a $Nd_3Cl_3[WO_6]$ single crystal and powder patterns for the derivatives of $Ln_3Cl_3[WO_6]$ with *Ln* = Pr, Nd, Sm – Tb.

Acknowledgements

The authors would like to thank *Dr. Sabine Strobel* for carrying out the diffuse reflectance spectroscopy measurements with the fluorescence spectrometer of *Prof. Dr. Wolfgang Kaim* (Institute for Inorganic Chemistry, University of Stuttgart, Germany). Furthermore, the finan-

cial support from the State of Baden-Württemberg (Stuttgart, Germany) is gratefully acknowledged.

Keywords: Chlorine; Tungsten; Lanthanides; Solid-state reactions; Structure elucidation

References

[1] S. Laufer, S. Strobel, Th. Schleid, J. Cybinska, A.-V. Mudring, I. Hartenbach, *New J. Chem.* **2013**, *37*, 1919–1926.
[2] T. Schustereit, Th. Schleid, H. A. Höppe, K. Kazmierczak, I. Hartenbach, *J. Solid State Chem.* **2015**, *226*, 299–306.
[3] G. Blasse, B. C. Grabmeier, *Luminescent Materials*, Springer-Verlag, Berlin, Heidelberg, **1994**.
[4] Th. Schleid, I. Hartenbach, *Z. Kristallogr.* **2016**, *231*, 449–466.
[5] G. Blasse, *Struct. Bonding (Berlin)* **1980**, *42*, 1–41.
[6] L. H. Brixner, H.-Y. Chen, C. M. Foris, *J. Solid State Chem.* **1982**, *45*, 80–87.
[7] L. H. Brixner, H.-Y. Chen, C. M. Foris, *Mater. Res. Bull.* **1982**, *17*, 1545–1556.
[8] G. Blasse, G. Bokkers, B. J. Dirksen, L. H. Brixner, *J. Solid State Chem.* **1983**, *46*, 215–221.
[9] G. Blasse, L. H. Brixner, *J. Solid State Chem.* **1983**, *47*, 368–372.
[10] T. Schustereit, Th. Schleid, I. Hartenbach, *Solid State Sci.* **2015**, *48*, 218–224.
[11] T. Schustereit, Th. Schleid, I. Hartenbach, *Z. Naturforsch. B* **2011**, *66*, 763–770.
[12] A. F. Holleman, E. Wiberg, *Lehrbuch der Anorganischen Chemie*, Walter de Gruyter, Berlin, New York, **1995**.
[13] V. A. Efremov, A. V. Tyulin, V. K. Trunov, *Kristallografiya* **1984**, *29*, 673–676.
[14] T. M. Polyanskaya, S. V. Borisov, N. V. Belov, *Dokl. Akad. Nauk SSSR* **1969**, *187*, 1043–1046.
[15] L. H. Brixner, H.-Y. Chen, C. M. Foris, *J. Solid State Chem.* **1982**, *44*, 99–107.
[16] G. Blasse, B. J. Dirksen, L. H. Brixner, *J. Solid State Chem.* **1982**, *44*, 162–168.
[17] J. B. Parise, L. H. Brixner, E. Prince, *Acta Crystallogr., Sect. C* **1983**, *39*, 1326–1328.
[18] C. Cascales, E. Antic-Fidancév, M. Lemaître-Blaise, P. Porcher, *J. Solid State Chem.* **1990**, *89*, 118–122.
[19] C. Cascales, E. Antic-Fidancév, M. Lemaître-Blaise, P. Porcher, *Eur. J. Solid State Inorg. Chem.* **1991**, *28*, 93–96.
[20] K. V. Dorn, Th. Schleid, I. Hartenbach, *Z. Anorg. Allg. Chem.* **2016**, *642*, 1045–1045.
[21] I. Hartenbach, F. Ledderboge, Th. Schleid, *Z. Kristallogr.* **2009**, *Suppl. 29*, 5.
[22] W. Herrendorf, H. Bärnighausen, *HABITUS*: Program for the Optimization of the Crystal Shape for Numerical Absorption Correction in *X-SHAPE* (version 1.06, Fa. Stoe, Darmstadt 1999), Karlsruhe, Gießen, **1993**, **1996**.
[23] G. M. Sheldrick, *Acta Crystallogr., Sect. A* **2008**, *64*, 112–122.
[24] T. Hahn, A. J. C. Wilson, *International Tables for Crystallography*, Kluwer Academic Publishers, Boston, Dordrecht, London, 2. ed., **1992**.
[25] B. Lafuente, R. T. Downs, H. Yang, N. Stone, *The Power of Databases: The RRUFF Project in Highlights in Mineralogical Crystallography*, Walter De Gruyter, Berlin, **2015**.
[26] C. Cascales, R. Sáez-Puche, P. Porcher, *J. Solid State Chem.* **1995**, *114*, 52–56.
[27] W. T. Carnall, P. R. Fields, K. Rajnak, *J. Chem. Phys.* **1968**, *49*, 4450–4455.
[28] G. H. Dieke, *Spectra and Energy Levels of Rare Earth Ions in Crystals*, Interscience Publishers, New York, **1969**.
[29] W. T. Carnall, P. R. Fields, K. Rajnak, *J. Chem. Phys.* **1968**, *49*, 4447–4449.
[30] W. G. Penney, R. Schlapp, *Phys. Rev.* **1932**, *41*, 194–207.
[31] J. H. van Vleck, *The Theory of Electric and Magnetic Susceptibilities*, Calendron Press, Oxford, **1932**.
[32] P. Dorenbos, *J. Lumin.* **2007**, *122–123*, 315–317.
[33] S. Cie, WinXPow: Program for Handling and Refinement of Powder Diffraction data, Darmstadt, **2001**.
[34] T. Roisnel, J. Rodriguez-Carvajal, WinPLOTR: a Windows Tool for Powder Diffractions Patterns Analysis, in *Mater. Sci. Forum, Proceedings of the Seventh European Powder Diffraction Conference EPDIC 7*, R. (Eds.: Delhez, E. J. Mittemeijer), Barcelona, 118–123, **2000**.
[35] W. W. Wendlandt, H. G. Hecht, *Reflectance Spectroscopy*, Interscience Publishers, New York, **1966**.
[36] G. Kortüm, *Reflectance Spectroscopy*, Springer, Berlin, New York, **1969**.
[37] N. J. Yamashita, *Phys. Soc. Jpn.* **1973**, *35*, 1089–1097.